Competition of Charge-Mediated and Specific Binding by Peptide-Tagged Cationic Liposome-DNA Nanoparticles *In Vitro* and *In Vivo*

Emily Wonder[1], Lorena Simón-Gracia[2], Pablo Scodeller[2,3], Ramsey Majzoub[1,4], Venkata Ramana Kotamraju[3], Kai K. Ewert[1], Tambet Teesalu[2,3*], and Cyrus R. Safinya[1*]

[1]University of California at Santa Barbara, Santa Barbara, California 93106

[2]University of Tartu, Ravila 14b, 50411 Tartu, Estonia

[3]Sanford-Burnham-Prebys Medical Discovery Institute, 10901 North Torrey Pines Road, La Jolla, California 92037

[4]Present address: Janssen Research & Development LLC, Spring House, Pennsylvania 19477

*Corresponding authors contact information: safinya@mrl.ucsb.edu, tteesalu@sbpdiscovery.org

Keywords

cationic liposome-DNA nanoparticles, tumor-penetrating peptides, iRGD, cyclic RGD, C-end Rule motif

Abstract

Cationic lipid vectors can be used as a modular gene delivery system that allows for easy tuning of the physicochemical properties that dictate cellular interactions and influence the delivery of exogenous nucleic acids. Cationic lipid-nucleic acid (CL–NA) complexes form spontaneously and can be sterically stabilized via PEGylation [PEG: poly(ethylene glycol)]. These PEGylated CL–NA nanoparticles (NPs) are also protected from opsonization in vivo and can be targeted to specific tissue and cell types via the conjugation of an affinity ligand. To achieve efficient targeting, it is necessary to maximize specific (receptor-ligand) binding and to suppress non-specific (electrostatic) interactions. Here, we use our library of PEG–lipids targeted with a panel of tumor-homing peptides to assess the *in vitro* and *in vivo* targeting abilities of tunable CL–NA nanoparticles. With modular CL–NA NPs, we can easily adjust ligand properties (i.e., binding motif and density) as well as charge properties (i.e., charge ratio and density), allowing for modulation of specific and non-specific binding interactions. Flow cytometry was used to quantitatively assess binding and internalization of NPs in cultured cancer cells. *In vivo* tumor selectivity of selected NP formulations was evaluated in a mouse model of peritoneal carcinomatosis of gastric origin. CL–NA NPs targeted with iRGD and cyclic RGD, as well as non-targeted NPs, were injected intraperitoneally, and biodistribution and tumor penetration were assessed by *ex vivo* macroscopic imaging and confocal microscopy. The CL–NA NPs showed tumor binding and minimal accumulation in healthy control tissues. The NPs preferentially bound to and penetrated the smaller tumor nodules, most similar to those known to drive recurrence of the peritoneal cancer in human patients. This study provides a starting point for tuning charge and ligand properties of CL–NA NPs to minimize off-target electrostatic binding and maximize ligand-receptor binding for efficient solid tumor targeting.

1. Introduction

Delivery of therapeutic nucleic acids with nanoscale carriers for the treatment of diseases involving misregulated or defective genes is an important, yet only partially achieved, goal [1–10]. Viruses are the conventional choice for gene vectors and account for a large majority of ongoing human gene therapy clinical trials [1]. However, viral vectors suffer from safety concerns and from limited loading capacity due to finite capsid size. Clinical applications of engineered retroviral and adenoviral vectors has resulted in cancer in two patients (probably due to insertional mutagenesis) and in severe immune reactions resulting in two deaths [11–13]. Synthetic delivery vectors, including those based on lipids or polymers, are investigated as a safer alternative. Lipid-based vectors allow for easy tuning of the physicochemical properties relevant for safe and controlled delivery of nucleic acids. The major challenges for synthetic vectors are improving their transfection efficiency and specificity profile, which are inferior to those of viral vectors [2–7].

Cationic liposomes (CLs) can be mixed with DNA or RNA, leading to the spontaneous formation of collapsed cationic lipid-nucleic acid (CL–NA) condensates with liquid crystalline phases. Most common is a multilamellar structure (L_α^C), with alternating layers of DNA and cationic lipid bilayers (Figure 1A) [14,15]. Different CL–NA nanostructures, created using lipids with different spontaneous curvatures, interact differently with cellular membranes, affecting membrane fusion and transfection efficiency. Another factor affecting the transfection efficiency by CL–NA complexes is charge density (σ_M), a predictive parameter for transfection by L_α^C CL–NA complexes *in vitro* [16,17]. Another key parameter, charge ratio (ρ_{ch}, the ratio of positive lipid charge to negative nucleic acid charge), shifts the optimal σ_M of the complexes [18]. Lipid-based gene delivery *in vivo* is challenging due to short circulation lifetime due to clearance of cationic liposomal carriers by cells of the reticuloendothelial system and the lack of selectivity in the binding of carriers towards desired cells and tissue types [19,20]. The former can be mitigated by adding PEG–lipids [PEG: poly(ethylene glycol)] to liposomes with the polymer chains in the brush state (e.g., 10 mol % for 2000 M_w PEG or 5 mol % for 5000 M_w PEG), creating a hydrophilic corona that stabilizes the complex into a nano-sized particle [21–24] and extends the circulation lifetime by limiting non-specific protein binding and NP blood clearance (Fig. 1A) [25–29]. Specific targeting can be attainable by attachment of affinity ligands (e.g., peptides, antibodies) that selectively interact with molecules s expressed on the target cells or tissue (Fig. 1) [19,20,30,31]. The NP surface functionalization with homing peptide–PEG–lipid provides a combination of affinity targeting and steric stabilization for precision guided delivery. Homing peptides have small size (and thus straightforward synthesis, eliminating the need for antibody protein engineering), low immunogenicity, low cost, biocompatibility, and moderate affinity that circumvents the affinity site barrier. Small homing peptides are particularly relevant in the context of nanoparticles, where even

small molecule targeting ligands with weak affinity can, through multivalent interactions, significantly enhance target-specific avidity (by up to 4 orders of magnitude), and thus the affinity of the final material is readily tunable. Numerous homing peptides have been identified using in vivo phage display [32–34], allowing targeting of a variety of disease states and normal tissues [35,36]. Some homing peptides confer additional therapeutically valuable properties such as membrane or tissue penetration [37,38]. In this study, we focused on the RGD and C-end Rule (CendR, R/KXXR/K) binding motifs, which bind to integrins and NRP-1, respectively. Both of these receptors are commonly overexpressed in cultured tumor cell lines and in tumor-derived cell populations *in vivo*, making them useful for developing smart cancer-seeking NPs [39–41]. We tested linear and cyclic versions of RGD-containing peptides[42,43]. The linear RGD peptide (GRGDSP) binds to multiple integrins but uses $\alpha_5\beta_1$ integrin as its preferred receptor [44]. Cyclic RGD peptides, like the c(RGDfK) used in this work[45,46], are conformationally restricted and bind more selectively and tightly than linear RGD peptides. These cyclic peptides can selectively target specific integrins such as the $\alpha_v\beta_3$ integrin that is overexpressed in many tumors [40,41]. RPARPAR, a linear prototypic CendR peptide, binds to both NRP-1 and NRP-2 , triggering cellular internalization, extravasation, and tissue penetration of the peptide and coupled payloads [47,48]. iRGD (CRGDKGPDC) uses α_v integrins for tumor recruitment and is processed by tumor proteases to expose a cryptic CendR motif (RGDK) to trigger NPR-1 binding. Such dual binding actuates tumor-specific extravasation and accumulation of iRGD [47,49–57]. In a recent study, we have demonstrated that iRGD- and RPARPAR-conjugated polymersomes loaded with paclitaxel show enhanced targeting and antitumor activity in mouse models of peritoneally disseminated tumors [38].

The goal of the current study was to assess the feasibility of targeting CL–NA NPs using homing peptides rather than the conventional antibody ligands. We have previously described three methods of preparing peptide–PEG–lipids and demonstrated their use in stabilizing CL–NA complexes into nanoparticles, targeting the NPs to cancer cell lines, and inducing cell internalization [31]. Here, we use a panel of peptide–PEG–lipids (Fig. 1B) to study tumor-targeting of the tunable CL–NA nanoparticles *in vitro* and *in vivo*. The targeting of tissues with homing peptides is complicated by the presence of non-specific interactions between the cationic lipids and anionic cellular membranes, which can be controlled by the charge ratio of the CL–NA complex. To explore the parameters controlling specific peptide-receptor binding (i.e., peptide, ligand-tagging density) and non-specific electrostatic binding (i.e., charge ratio), a wide range of formulations needs to be tested, making the *in vivo* evaluation of all formulations expensive and time-consuming. Therefore, we decided to first assess *in vitro* cell binding and uptake using flow cytometry. We looked for high cellular binding of the targeted (homing peptide-tagged) NPs and low binding of the equivalent non-peptide NPs. Two different cancer cell lines PC3 (prostate

cancer) and M21 (melanoma) were used, with M21 lacking the NRP-1 (CendR target) receptor. Based on the *in vitro* assessment of cell binding, two formulations were selected for *in vivo* testing.

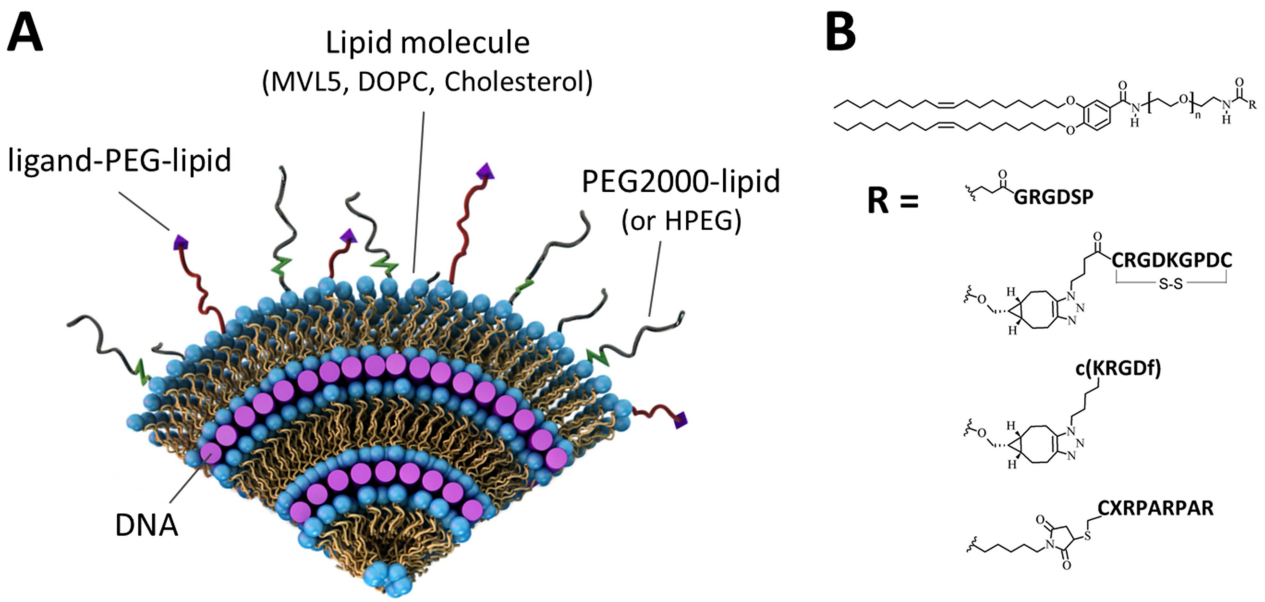

Figure 1 (A) A surface-modified cationic liposome–DNA nanoparticle (CL–NA NP), composed of cationic lipid bilayers with negatively charged nucleic acids (purple rods) in a lamellar liquid crystal structure and modified with polymer−lipid molecules forming a polymer corona. Surface properties of the NP can be optimized for *in vivo* delivery using hydrophilic polymers (e.g., poly(ethylene glycol), PEG). These polymers provide steric repulsion which stabilizes the complex into a nanoparticle of well-defined size and inhibits nonspecific protein binding and opsonization by the immune system. Targeted delivery can also be achieved by the addition of cell-targeting ligands (purple triangles) to the distal end of the polymer− lipid. Acid-labile polymer−lipids (HPEG) can be used to release the polymer in low-pH late endosomes, promoting interactions between cell and nanoparticle membranes. Adapted and modified with permission from ref 3. Copyright 2014, RSC Publishing. (B) Chemical structure of peptide–PEG–lipid molecules used to provide targeting for CL–NA NPs. A PEG2000–DOB building block is conjugated with a peptide (linear RGD, iRGD, cyclic RGD, or linear RPARPAR) via solid phase synthesis, thiol-maleimide conjugation, or copper-free 'click' chemistry [31]. In all cases, PEG MW= 2000 g/mol (n=45) and DOB is 3,4-Di(oleyloxy)benzoic acid. For the RPARPAR–PEG–lipid, X represents 6-Azido-hexanoic acid, which was conjugated to the N-terminus of the RPARPAR peptide (on resin).

For *in vivo* testing, we used a mouse model of gastric cancer (MKN-45P) which, like clinical gastrointestinal and gynecological cancers, spreads in the peritoneal cavity, forming disseminated tumors (known as peritoneal carcinomatosis, PC) [58]. Clinically, after surgical resection of the primary tumors (cytoreduction), microscopic tumor nodules and disseminated cancer cells that remain in the peritoneal cavity may grow into new tumors, resulting in cancer recurrence [58–61]. To eliminate the cancer cells remaining after surgery, locoregional intraperitoneal (IP) chemotherapy is increasingly used to achieve elevated drug concentration in the IP space and to decrease systemic exposure [58,61,62]. Despite these advances, 60% of PC patients still experience cancer recurrence [63]. We have demonstrated that the therapeutic efficacy of IP polymeric nanoparticles can be improved by targeting with the iRGD peptide [38]. Here, we evaluated the effect of homing peptide functionalization on the tropism of CL–NA NPs. First we used *in vitro* testing to audition CL–NA NPs of different electrostatic properties to optimize *in vitro* selectivity of the NPs. The selected NPs were injected IP into mice with MKN-45P gastric tumors. Biodistribution and tumor penetration were assessed using *ex vivo* whole-organ imaging and confocal imaging of sectioned tumor tissue, respectively. Targeted NPs were found to have very good tumor-homing and showed low accumulation in non-malignant control tissues. Untargeted CL–NA NPs also showed preferential accumulation in tumor tissue, potentially due to electrostatics or size of the NPs, and properties of tumor tissue. We found that NPs preferentially bound to and penetrated the smaller tumor nodules, a highly clinically relevant target known to drive recurrence of the cancer after cytoreductive surgery.

2. Materials/Methods

2.1. Materials

DOPC was purchased from Avanti Polar Lipids as a solution in chloroform. Pentavalent MVL5, PEG2000–lipid, RGD−, iRGD−, cRGD−, and RPARPAR−PEG2000−lipid were synthesized as previously described [31,64,65]. The pGFP plasmid encoding the GFP gene was purchased from Promega, propagated in Escherichia coli and purified using Qiagen Giga or Mega Prep kits. Stock solutions of pGFP were prepared in deionized water (dH_20). For in vitro studies, the pGFP was labeled using YOYO-1 dye (Molecular Probes). For *in vivo* studies, the pGFP plasmid was labeled using the Mirus Bio Label IT Nucleic Acid Labeling Kit with Cy5 (excitation/emission maximum: 649 nm/670 nm).

2.2. Liposome and DNA Preparation

Stock solutions of MVL5 and PEG2000-lipid were prepared by dissolving them in a 3:1 chloroform/methanol mixture. RGD−, iRGD−, and cRGD−PEG2000−lipid were dissolved in a 65:25:4 chloroform/methanol/dH20 (dH20,

deionized water) v/v/v mixture. RPARPAR−PEG2000−lipid was dissolved in methanol. These lipid solutions were combined at the desired molar ratio. All compositions investigated had 10 mol % MVL5 and total of 10 mol % PEG2000−lipid and peptide (RGD, iRGD, cRGD, RPARPAR)−PEG2000−lipid, where the lipid tail is DOB (3,4-Di(oleyloxy)benzoic acid). After mixing the lipid solutions, the organic solvent was evaporated by a stream of nitrogen followed by incubation under vacuum overnight (12−16 h). The appropriate amount of high resistivity water (18.2 MΩcm) was added to the dried lipid film to achieve the desired lipid concentration (1 mM). Hydrated films were incubated overnight at 37 °C to form liposomes. The liposome solution was then sonicated for 7 minutes using a tip sonicator to promote the formation of small unilamellar vesicles. Plasmid purification was performed according the manufacturers protocol. For *in vitro* experiments, pGFP was labeled with YOYO-1, using a dye/basepair ratio of 1:30 by incubating the appropriate amounts of dye and pGFP at 37 °C overnight. For *in vivo* experiments, pGFP was labeled using Cy5 according to the manufacturer's protocol with one modification: the incubation time at 37 °C was increased from 1 to 2 h to improve labeling efficiency. To form CL–NA complexes, the unilamellar vesicles were mixed with labeled DNA, and they self-assembled into fluorescent multilamellar nanoparticles [8].

2.3. Membrane Charge Density and Charge Ratio

For the composition used in this study (10/70/10/10, molar ratio of MVL5/DOPC/Cholesterol/x, with x = PEG−lipid and/or peptide (RGD, iRGD, cRGD, RPARPAR)−PEG−lipid), the membrane charge density was low, $\sigma_M \approx 0.0061$ e/Å^2. The membrane charge density can be calculated from the equation $\sigma_M = [1 - \Phi_{nl}/(\Phi_{nl} + r\Phi_{cl})]\sigma_{cl}$. Here, $r = A_{cl}/A_{nl}$ is the ratio of the headgroup areas of the cationic and the neutral lipid; $\sigma_{cl} = eZ/A_{cl}$ is the charge density of the cationic lipid with valence Z; Φ_{nl} and Φ_{cl} are the molar fractions of the neutral and cationic lipids, respectively. In the calculation, the neutral lipid component consists of the sum of DOPC, cholesterol, and the PEG−lipid (with and without peptide). The membrane charge density was calculated using $A_{nl} = 72$ Å2, $r_{MVL5} = 2.3$, and $Z_{MVL5} = 5.0$. Another key parameter, charge ratio, ρ_{ch}, indicates the molar ratio of positive lipid charge to negative DNA charge in the liposome and DNA solutions that are mixed to form CL–NA NPs. The nanoparticles studied here were prepared at charge ratios of 0.5, 1.0, 1.2, 1.5, or 5. The isoelectric point (neutral surface charge) of MVL5-based CL–NA complexes has been previously found to be at a charge ratio (ρ_{ch}) between 1.0 and 1.5.

2.4. Cell Culture

PC-3 cells (ATCC number: CRL-1435; human prostate cancer) and M21 human melanoma cells (gift from David Cheresh) were cultured in DMEM (Invitrogen) supplemented with 10% fetal bovine serum (Gibco) and 1%

penicillin/streptomycin (Invitrogen). Cells were passaged every 72 h to maintain subconfluency and cultured in an incubator at 37 °C in a humidified atmosphere containing 5% CO_2. MKN-45P human gastric cancer cells were originally isolated from parental MKN-45 cells (gift from Joji Kitayama) as described in [66]. The MKN-45P cells were cultivated in DMEM (Lonza, Belgium) containing 100 IU/mL of penicillin and streptomycin, and 10% of heat-inactivated fetal bovine serum (GE Healthcare, UK).

2.5. Flow Cytometry

Cells were detached using enzyme-free cell dissociation buffer (Gibco), seeded in 24-well plates at a density of 45 000 cells/well, and incubated for 18 h. A total of 1µg of pGFP (10% YOYO-1–labeled) was used for each sample (duplicate wells). The DNA was diluted to 250 µL with DMEM. The appropriate volume of liposomes (to reach the desired lipid/DNA charge ratio) was also diluted to 250 µL with DMEM. The diluted liposome and DNA solutions were mixed and incubated at room temperature for 20 minutes to allow nanoparticle formation. After washing the cells with PBS, 200 µL of NP solution was added to each well. Control wells received only DMEM or only (labeled) DNA. Cells were incubated with nanoparticles for 5 hr, rinsed with PBS, detached with enzyme-free cell dissociation buffer (Gibco), and suspended in 200 µL of DMEM. Cells were maintained on ice after harvesting to inhibit further uptake of NPs during the measurement. Fluorescence was measured using a Guava EasyCyte Plus Flow Cytometry System (Millipore). Cell solutions were passed through a 100 µm filter to disperse aggregates prior to measurement. The filtered cell solution was divided in two. One half was mixed with a Trypan Blue solution (0.4% in water, Gibco) at a 4:1 (cell:TB) v/v ratio and incubated for 5–10 minutes before the measurement, quenching extracellular fluorescence. The other half of the cell solution was mixed with PBS at the same 4:1 v/v ratio and measured immediately. The software parameters were set such that 10,000 events constituted a single measurement, though some samples with significant cell detachment only reached ~2,000 event before time expired on the measurement. The flow cytometry results were analyzed using the Cyflogic software (CyFlo Ltd). Events were sorted using forward and side scattering to separate cells from debris. A single acceptance window was used for each plate of cells, taking care to account for any shifting of the scattering due to high NP binding. The green fluorescence distribution of the accepted events (cells) was log-normal, making the geometric mean a more accurate measure of the distribution than the arithmetic mean. The coefficient of variation (CV) of the fluorescence distribution was used to calculate the uncertainty in the geometric mean using the following equation: $\sigma_{ERROR} = \log(CV^2 - 1) \times I / N$, where I is the geometric mean and N is the number of counted cells. The geometric mean was then normalized by subtracting the geometric mean of the control cells' autofluorescence. The propagated uncertainty of the mean NP fluorescence included the error of both the total fluorescence and control autofluorescence distributions.

2.6. In vivo biodistribution studies

Athymic nude mice were purchased from Harlan Sprague Dawley Inc. All the animal experimentation protocols were approved by Estonian Ministry of Agriculture, Committee of Animal Experimentation (Project #42). Mice were injected intraperitoneally (IP) with 2×10^6 MKN-45P cells, and the MKN-45P tumors were allowed to grow for two weeks. CL–NA NPs containing Cy5-labeled pGFP were injected IP (0.1 mL of 5 mg/mL solution was diluted in 0.5 mL of PBS). After 24 h, the animals were perfused with 10 mL of PBS. The tumors and organs were excised for the fluorescence visualization using an Optix MX3 (Advanced Research Technologies). Fluorescence quantification was done using the OptiView analysis software. The average fluorescent signal (n=3) was normalized by the control mouse (receiving no injection) and divided by the total grams of tissue. Tissues were snap-frozen in liquid nitrogen and stored at –80°C for further analysis.

2.7. Immunofluorescence and microscopic imaging

The snap-frozen tumors and organs were cryosectioned at thickness of 10 µm and fixed with 4% of paraformaldehyde in PBS. To visualize expression of exogenous pGFP delivered by our NPs, the tissue was immunostained with anti-GFP rabbit IgG (Novus Biologicals) as the primary antibody and Alexa 546-conjugated goat anti-rabbit IgG (Molecular Probes) as the secondary antibody. The nuclei of cells were counterstained with 1 µg/ml DAPI. The pGFP DNA was conjugated with a Cy5 label, allowing for fluorescence imaging of the NPs. Tissue sections were imaged on a Zeiss LSM 510 and an Olympus FV1200MPE. Confocal images of the tissue sections were analyzed with the ZEN lite 2012 and Olympus FluoView image software, respectively. The fluorescence from the NPs was quantified using Image J software.

3. Results

3.1. In vitro uptake and internalization of peptide-tagged NPs

The binding and internalization of CL–NA NPs by cancer cell lines was assessed using flow cytometry. PC-3 and M-21 cells were incubated with CL–NA NPs loaded with YOYO-1–labeled pGFP for 5 hours. The cell-associated fluorescence was measured with and without added Trypan Blue, a dye that quenches extracellular fluorescence, to distinguish total cell-bound and internalized nanoparticle fractions. The nanoparticles were formulated at ρ_{ch} = 0.5, 1.0, 1.2, 1.5, or 5 with lipid mixtures of 10/70/10/10-x/x MVL5/DOPC/Cholesterol/PEG2000–lipid/y, where x=1, 2.5, 5, and 10) and y=PEG2000–lipid, RGD–, iRGD–, cRGD–, or RPARPAR–PEG2000–lipid. The charge ratio affected surface charge and non-specific electrostatic interactions, whereas peptide structure and its density affected specific binding. RGD, iRGD, and cRGD all

contain the integrin-binding RGD motif and bind to both PC-3 and M-21 cell lines, which overexpress α_v integrins [67,68]. iRGD and RPARPAR contain the CendR motif (R/KXXR/K) that targets NRP-1 which is overexpressed on the PC-3 cells and absent on the M21 cells. Figure 2 shows flow cytometry-based analysis of binding of NPs at ρ = 1.5 (near neutral surface charge) with peptide–PEG–lipids at 1, 2.5, 5, and 10 mol %. Binding and internalization of the NPs was in most cases higher than internalization alone, indicating that a significant portion of NPs are bound to the outside of the cells. Generally, PC-3 cells showed lower internalization than M-21 cells. Cells incubated with cRGD-tagged NPs (with >1 mol% cRGD-PEG-lipid) had high rates of detachment from the cell culture dish. In detached cells, we observed elevated cRGD-NP binding but no effect on internalization ("cRGD (det.)" in Fig. 2). For the cells that remained attached, cRGD-tagged NPs generally showed higher binding and a higher fraction of internalization than NPs targeted with other peptides. Naked DNA did not bind and was not internalized. The non-targeted control PEG NPs showed lower binding and internalization than the targeted peptide-tagged NPs, with the exception of some NPs with full peptide-coverage (10 mol%).

NPs targeted with RPARPAR showed specificity to the NRP-1 receptor at 2.5 mol% peptide, where the total binding of NP to PC-3 cells was twice as high as binding to M-21 cells. Unexpectedly, the binding and internalization of NPs targeted with RPARPAR was very similar in both PC-3 and M-21 cell lines for very low (1 mol%) and high (5-10 mol%) peptide coverage, despite the fact that M-21 cells are negative for the expression of NRP-1. This suggests that under conditions tested, non-specific charge interactions from the cationic RPARPAR peptide (net +2 charge with C-terminal acid) are important for binding and internalization. Because the cell interactions of CL–NA NPs are very sensitive to charge, the addition of many cationic RPARPAR peptides (>5 mol%) to the surface of the NP resulted in high non-specific electrostatic binding.

The density of targeting ligand also affects NP interaction with the cells. For PC-3 cells, the total binding and internalization of peptide-tagged NPs increased from 1 to 2.5 mol% peptide, then slowly dropped off for 5 and 10 mol% peptide. For M-21 cells, the total binding and internalization increased from 1% up to 5 mol% peptide and dropped at 10 mol% peptide. The effect of peptide density on the interaction of peptide-NPs with the cells appeared also to depend on the targeting peptide used, i.e. binding and internalization was highest at 2.5 mol% RGD–PEG–lipid and at 5 mol% iRGD–PEG–lipid. Overall, the highest binding and internalization was observed at 2.5 or 5 mol% peptide, depending on the cell line and peptide. At 10 mol% peptide, there is a significant drop in binding and internalization of most peptide-tagged NPs. The binding of RPARPAR-targeted NPs peaks at 2.5 mol% for PC-3 and 5 mol% for M-21, with the peak binding to PC3 being ~30% higher. This is to be expected given that the M-21 binding is purely non-specific electrostatic attraction, while the PC-3 binding is a combination of both specific and non-specific binding.

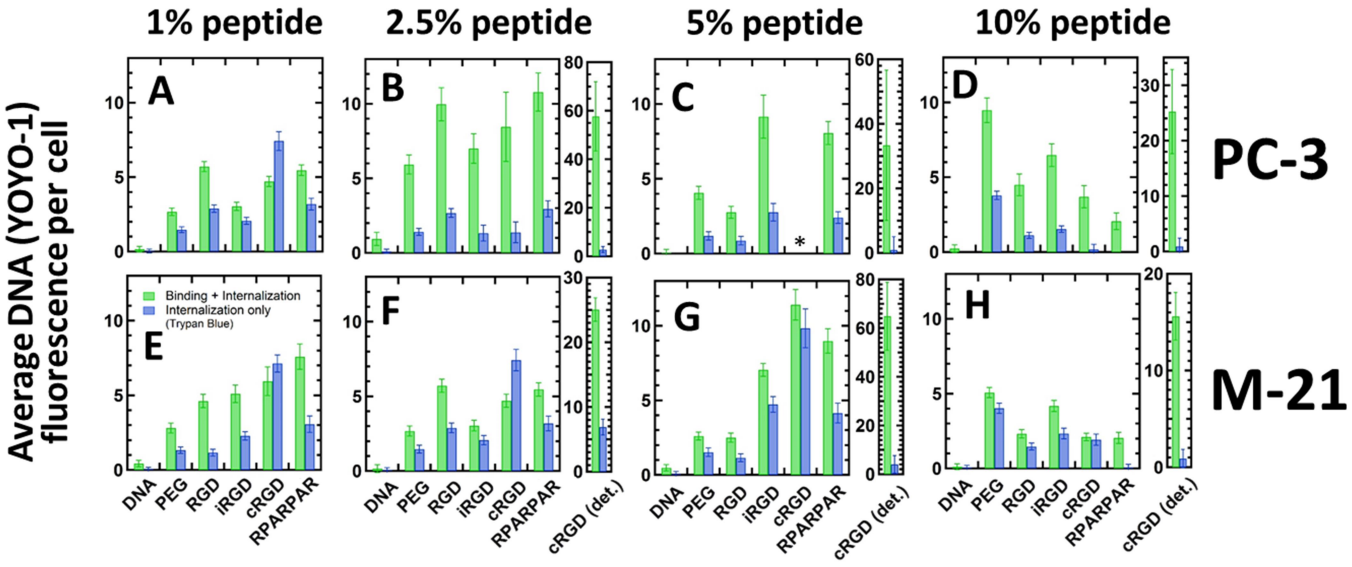

Figure 2 Flow cytometry measurements of binding and internalization as a function of peptide density. PC-3 (A-D) and M-21 (E-H) cells were incubated for 5 h with nanoparticles containing labeled DNA or labeled DNA only. The nanoparticles were formulated at ρ = 1.5 with lipid mixtures of 10/70/10/10-x/x MVL5/DOPC/Cholesterol/PEG2000–lipid/y, where x=1 (A,E), 2.5 (B,F), 5 (C,G), and 10 (D,H) and y=PEG2000-lipid, RGD-, iRGD-, cRGD-, or RPARPAR-PEG2000-lipid. Fluorescence was measured with or without Trypan Blue (TB), which quenches external fluorescence. The geometric mean was normalized by subtracting the geometric mean of the control cell autofluorescence (no labeled DNA). Combined binding and internalization of NPs (green, without TB) and internalized NPs only (blue, with TB) are shown. For x>1, cRGD-tagged NPs caused significant cell detachment from the growth substrate (labeled "cRGD (det.)"). For x=5, too few attached PC3 cells remained to obtain data (*).

To probe the effects of electrostatic interactions of peptide-tagged NPs with cells, we measured binding and internalization as a function of charge ratio (ρ). For NPs with a fixed peptide density (2.5 mol%), we varied charge ratio (ρ) from 0.5 (anionic NPs) to 5 (highly cationic NPs). Figure 3 shows the total binding and internalization (A,D), internalization only (B,E), and the ratio of internalization only to total binding and internalization (C,F). As shown in Figure 3A and D, binding and internalization of all NPs tends to increase with charge ratio, with a plateau for $1 \leq \rho \leq 1.5$. PC-3 generally shows higher total binding and higher internalization for NPs of negative or neutral charge ($\rho \leq 1.5$), while M-21 has overall higher binding for the highly cationic NPs (ρ = 5), indicating that interactions with M-21 cells are more sensitive to NP charge. Again, the detached cells incubated with cRGD-tagged NPs showed much higher binding than the other samples (see dashed lines in Fig 3A inset & 3D). Cells incubated with RPARPAR-targeted NPs also show very high total cell binding and internalization in both cell lines. While internalization of the RPARPAR-targeted NPs by PC3 was very high, internalization by M-21 was low, similar to that of the non-targeted NPs, due to the absence of the NRP-1

receptor. Non-targeted control PEG NPs always have lower binding and internalization than the corresponding peptide-tagged NPs. However, the PEG NPs also showed increased binding and internalization with increased NP charge ratio. As a consequence, non-targeted PEG NPs at $\rho = 5$ (highly cationic) have higher binding and internalization than targeted peptide-tagged NPs at $\rho = 1.5$ (near neutral).

Similarly, Figures 3B and E show that internalization increased with charge ratio, with a plateau around $1 \leq \rho \leq 1.5$. Again, M-21 cells showed a faster increase than PC-3 cells. Detached cells incubated with cRGD-tagged NPs, despite having very high NP total binding and internalization, showed internalization very similar to that of the corresponding attached cells. RPARPAR-tagged NPs showed high internalization by PC3 cells, but very low internalization (comparable to non-targeted PEG NPs) by M21 cells lacking the NRP-1 (internalization comparable to non-targeted PEG NPs).

Fig 3C & 3F show the ratio of DNA internalization to total binding & internalization, roughly indicating the ratio of NPs that get internalized by the cell after binding (with a ratio of 1 indicating that all NPs that bind to the cell are internalized). There is not a clear trend for low charge ratios ($\rho = 0.5$ and 1.0). However, most NP formulations show a decrease in internalization ratio between $\rho = 1.2$ and 1.5 followed by a recovery at $\rho = 5$. The two exceptions to this are cRGD- and RPARPAR-tagged NPs incubated with M21 cells. RPARPAR-tagged NPs have low internalization ratios overall for M-21 cells, including the lowest internalization by a large margin at $\rho = 5$. On the other hand, cRGD-tagged NPs showed very high internalization ratios in attached M-21 cells, often exceeding a ratio of 1. Whereas this reveals limitations in this interpretation of the measurement, it does indicate that nearly all cRGD-tagged NPs were internalized by attached M-21 cells. Detached cells of both lines (PC-3 and M-21) incubated with cRGD-tagged NPs showed some of the lowest internalization ratios. This data also confirms the earlier observation that PC-3 cells internalize fewer NPs, as evidenced by the generally lower NP internalization ratios compared to M-21 cells. Based on these results, 5 mol% peptide density was chosen for subsequent *in vivo* studies to maximize specific binding. A moderate charge density, $\rho = 1.5$, was chosen to optimize specific binding relative to nonspecific (electrostatic) binding.

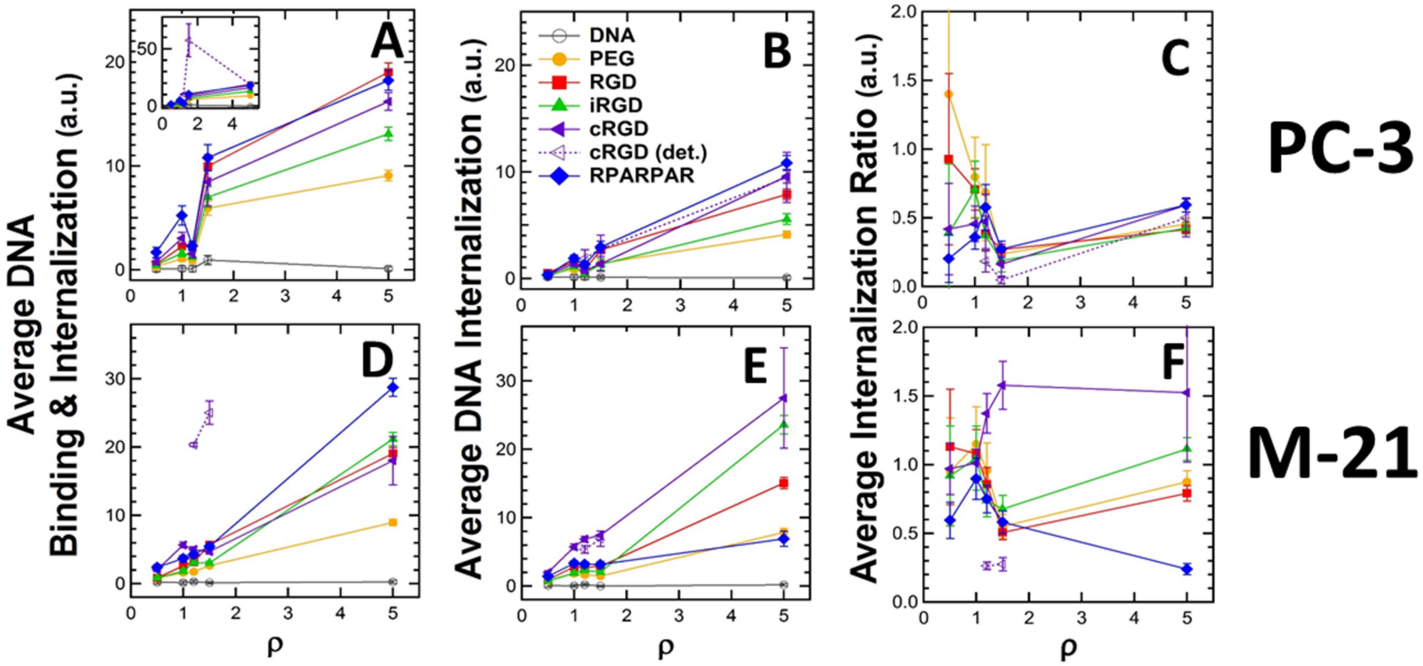

Figure 3 Flow cytometry measurements of binding and internalization as a function of charge ratio. PC-3 (A-C) and M-21 (D-F) cells were incubated for 5 h with nanoparticles containing labeled DNA or labeled DNA only. The nanoparticles were formulated at ρ = 0.5, 1.0, 1.2, 1.5, and 5 with lipid mixtures of 10/70/10/7.5/2.5 MVL5/DOPC/Cholesterol/PEG2000–lipid/x where x=PEG2000-lipid, RGD-, iRGD-, cRGD-, or RPARPAR-PEG2000-lipid. Green fluorescence was measured with or without trypan blue, which quenches extracellular fluorescence. The geometric mean was normalized by subtracting the control cells' autofluoresence (no labeled DNA), giving the mean YOYO-1 fluorescence per cell. (A,D) Combined binding and internalization of NPs. The inset shows detached cells treated with cRGD-tagged NPs, which have a much higher binding and internalization than the other samples. (B,E) Fluorescence of internalized NPs only. (C, F) Ratio of internalization only to combined binding and internalization. For x > 1, cRGD-tagged NPs resulted in cell detachment from the growth substrate. These cells were collected and measured separately (labeled "cRGD (det.)"). DNA with no carrier (naked DNA) is shown with open gray circles, control PEG NPs with no peptide are shown as filled orange circles, RGD-tagged NPs are marked as red squares, iRGD-tagged NPs are marked as green upright triangles, cRGD-tagged NPs are marked as purple rotated triangles, with attached cells shown as filled markers and detached cells shown as open markers, and RPARPAR-tagged NPs are marked as blue diamonds.

3.2. In vivo biodistribution

Mice bearing IP MKN-45P tumors were injected with three different NP compositions (n=3). In addition to the control PEG NP, we also tested iRGD- and cRGD-tagged NPs due to their high internalization by M-21 cells. Furthermore, iRGD has tumor-penetrating properties *in vivo* due to the *in situ* tumor exposure of the CendR (NRP-1–binding) motif by tumor-derived proteases. The fluorescent NPs were administered by IP injection, and 24h later, the tumors and control organs were excised and analyzed by macroscopic fluorescence imaging and

confocal analysis of the tissue sections. The fluorescence of the Cy5-labeled NPs was imaged also in the nonmalignant organs (Figure 4). For all NP formulations, the NP fluorescence was much higher in the tumor than in any other organs. Outside of the tumor, the highest NP accumulation was seen in the liver and lung. The low accumulation of NPs in healthy tissue was confirmed by confocal imaging of sectioned tissue (see Fig S1).

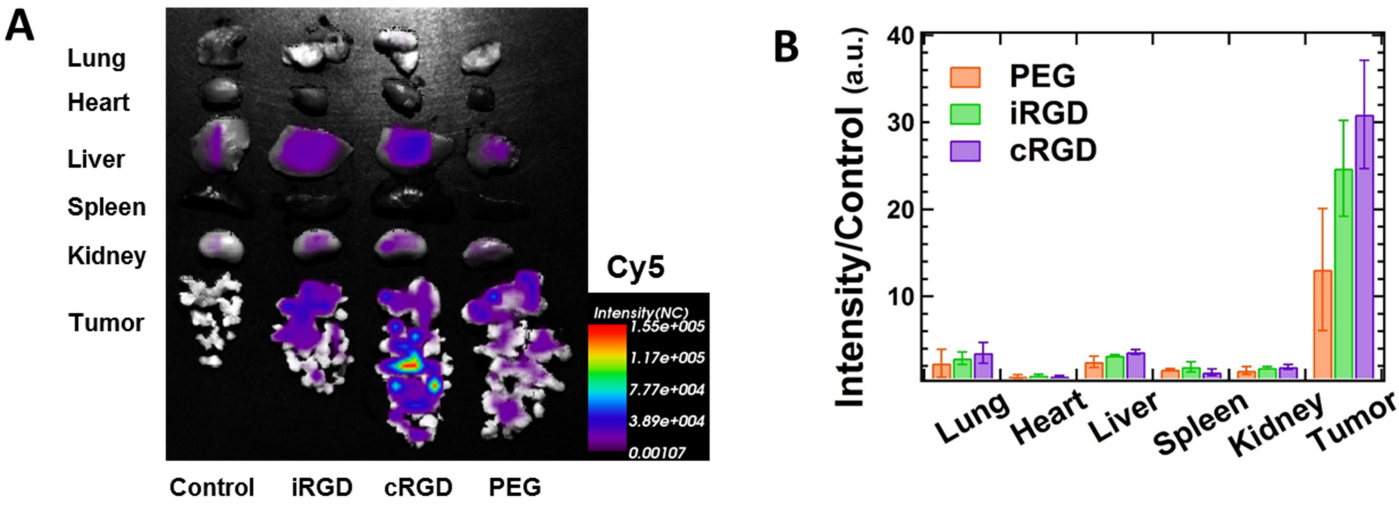

Figure 4 *Ex vivo* biodistribution of IP-administered CL–NA NPs. (A) Mice bearing IP MKN-45P tumors were IP injected with either PBS (control) or ~0.5 mg of CL–NA NPs of the composition 10/70/10/5/5 MVL5/DOPC/Cholesterol/PEG2K-lipid/x where x = PEG2K-lipid, iRGD-PEG2K-lipid, or cRGD-PEG2K-lipid with ρ = 1.5. After 24 h the tumors and organs of interest were excised and fluorescent signal from the Cy5-labeled DNA was imaged with Optix® MX3 (Advanced Research Technologies, Canada). Representative compound fluorescent and bright-field images from four independent experiments are shown. (B) Quantification of the *ex vivo* fluorescent signal in tumors and other organs by the Art Optix software. The fluorescence was normalized to the grams of tissue then averaged for the n=3 mice. This average was then divided by the autofluorescence of the control mouse (receiving no injection).

3.3. In vivo tumor penetration

To examine the distribution of the NPs in the tumor tissue, confocal imaging was used. First, tumor nodules were dissected free from the membranous tissue connecting the nodules. Then tumor nodules from all mice (n=3) were combined, snap-frozen, cryosectioned, and imaged. The resulting images are shown in Figure 5. All NP formulations showed some NP binding to the surface of the tumor nodules and superficial (10-20 μm) penetration. The iRGD- and cRGD-targeted NPs had a tendency to accumulate in small tumor nodules (diameter ~300 μm). The peptide-tagged NPs penetrated deeper (>100 μm) into these small tumor nodules, as shown in Figure 5D and 5F. GFP expression was fairly low in all samples, as we did not add components like ionizable lipids or acid-labile PEG–lipids (HPEG) [69] that would have aided in endosomal escape required for gene expression following cellular uptake of DNA-containing NPs.

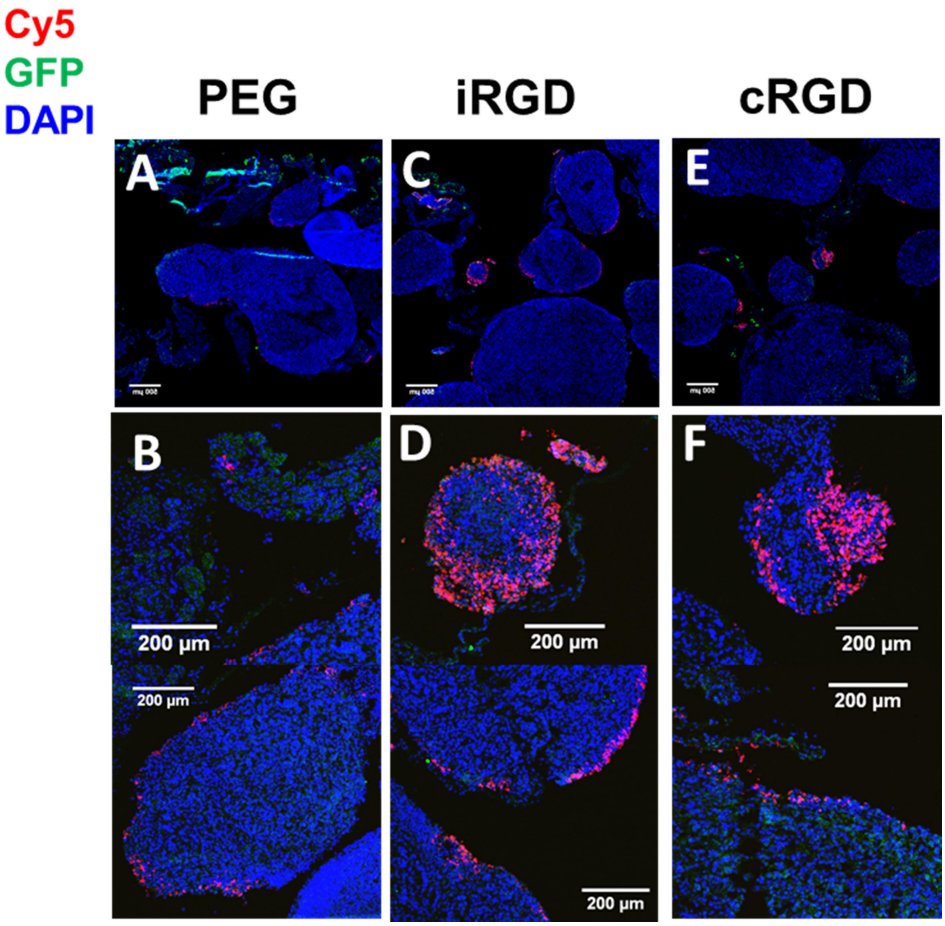

Figure 5 Confocal imaging of CL–NA NPs in tumor tissue. Fluorescence confocal images of tissue sections prepared from IP MKN-45P tumor nodules collected 24 h after IP injection of NPs. Tumor nodules from all n=3 mice were excised, separated from membranous tissue connecting the nodules, mixed together, sectioned, and imaged. Cy5 DNA-label is shown in red (NPs), anti-GFP immunofluorescence is shown in green (DNA expression), and DAPI is shown in blue (cell nuclei). All NPs had a formulation of 10/70/10/5/5 MVL5/DOPC/PEG2000-lipid/x where x=PEG2000-lipid, iRGD-, or cRGD-PEG2000-lipid with ρ =1.5. (A,B) Tumor nodules from mice treated with control PEG2000-lipid NPs. (C,D) Tumor nodules from mice treated with iRGD-tagged NPs. (E,F) Tumor nodules from mice treated with cRGD-tagged NPs. Samples were imaged on a Zeiss LSM 510, with scale bars of 500µm (A,C,E), and at a higher magnification on an Olympus FV1200MPE, with scale bars of 200µm (B,D,F). The Cy5-labeled NPs are found primarily on the surface of tumor nodules. (D,F) iRGD- and cRGD-tagged NPs can be seen to penetrate deeper into smaller tumor nodules (diameter ~ 300µm) and some higher-curvature surfaces of large tumor nodules.

4. Discussion

Our goal was to assess the feasibility of targeting CL–NA NPs *in vivo* using peptides as ligands, which, to our knowledge, has not been previously attempted. Effective tissue-targeting by CL–NA NPs requires both high

specific peptide-receptor binding and minimal non-specific binding between the cationic lipids and anionic cellular membranes. Controlling specific peptide-receptor binding involves both choice of ligand, in this case peptide, and the density of ligand on the surface of the particle. Non-specific binding of CL–NA NPs is primarily affected by the NPs surface charge, which can be easily modulated via the cationic lipid : nucleic acid charge ratio. To streamline the testing of these parameters, we used flow cytometry as an *in vitro* assessment of cell binding and uptake prior to *in vivo* testing. We hoped to identify three parameters: 1) the peptide with the highest binding to cancer cells, 2) the mole fraction of peptide–PEG–lipid that achieved the highest binding, and 3) the charge ratio that minimized non-specific electrostatic binding of the non-targeted (PEG) NPs while still allowing for adequate peptide-mediated cell binding. We used CL–NA NPs with a low membrane charge density (10% MVL5) to reduce nonspecific electrostatic attraction between the NP cationic membranes & anionic cellular membranes. We then measured binding and uptake for a variety of surface functionalizations and charge ratios.

We found that the peptide with the highest binding and internalization by both PC-3 (prostate cancer) and M-21 (melanoma) cells was cRGD. The binding of the optimized cyclic peptide by $\alpha_v\beta_3$ integrin was so strong that it appears to have been out-competing the tissue culture substrate, resulting in detachment of the cells from the growth surface. We found that the detached cells had very high total NP binding and internalization but moderate overall internalization, indicating that detachment from the substrate may have halted the internalization of NPs. Attached cells incubated with cRGD-tagged NPs showed very high internalization relative to total binding and internalization. The total combined binding and internalization of the RPARPAR-tagged NPs showed specificity to the NRP-1 receptor at low (2.5 mol%) peptide density, but not at higher peptide densities, likely due to non-specific electrostatic interactions between the cationic peptides and the plasma membrane. This non-specific binding is likely more prevalent than in previous studies of RPARPAR-targeted NPs due to our long incubation time (5 hr rather than 1 hr), which often results in increased non-specific binding. Internalization of RPARPAR-targeted NPs did show specificity to the NRP-1 receptor, with PC-3 cells showing very high internalization, and M-21 cells showing low internalization at the level of the control non-targeted NPs. This indicates that RPARPAR interaction with the cell surface can occur non-specifically in the absence of the NRP-1 receptor as a result of electrostatic attraction between the +2 charged peptide and anionic cellular membranes, but the internalization appears to be largely mediated by the NRP-1 receptor. This demonstrates the importance of considering the charge of peptide ligands when attempting to target specific tissues with NPs near neutral surface charge. Another CendR peptide, iRGD, showed binding and internalization lower than that of cRGD or RPARPAR, which is unsurprising given that the cryptic CendR motif is not exposed *in vitro*. The traditional linear RGD peptide did little to enhance NP binding and internalization in most cases.

Binding and internalization of NPs varied significantly with the density of peptide ligands. Peptide–PEG–lipids made up 1 to 10 mol% of the lipid mixture, with the total peptide–PEG–lipid and PEG–lipid concentration held at 10 mol%. We found that the optimal peptide–PEG–lipid density was not at full coverage (10 mol%) but instead generally at 2.5mol% for PC-3 cells and 5 mol% for M-21 cells, with a few exceptions. At 10 mol% peptide, there was a significant drop in binding and internalization of most peptide-tagged NPs. One possible explanation for this is that the addition of peptides to the end of all PEG chains resulted in a thicker hydrophilic corona around the NP, further decreasing electrostatic attraction.

We also varied NP charge ratio (positive lipid : negative DNA charge ratio), which effects the overall charge of the CL–NA complex. High charge ratios ($\rho > 1.5$) result in NPs with an overall positive surface charge, and low charge ratios ($\rho < 1$) result in NPs with an overall negative surface charge. We found that the total binding and internalization of all NPs increased with charge ratio. Important to note is that the binding and internalization of control PEG NPs, containing no peptide, also increased with charge ratio. Since binding and internalization of control PEG NPs is non-specific and likely mediated by electrostatics, we can use this as a rough measure of the degree of non-specific binding and internalization of our NPs by non-targeted tissues (i.e., healthy organs). Because of this, we expect that NPs with a high charge ratio may show higher off-target binding *in vivo* due to their increased surface charge.

We selected iRGD- and cRGD-tagged NPs with moderate charge ratio (ρ = 1.5) and moderate ligand density (5 mol%) to test in a mouse model of gastric cancer (MKN-45P). We found that targeted NPs injected intraperitoneally showed very good tumor-homing properties. Ex vivo imaging showed very high NP accumulation in the tumor and slight accumulation in the liver, much lower than is typical for nano-sized particles. The low but visible presence of peptide-tagged NPs in the lungs indicates that some NPs may have escaped the abdominal cavity and entered the bloodstream. The PEG control NPs also showed a preference for binding tumor tissue despite the lack of specific peptide-ligand binding, indicating its tumor-homing must be a result of non-specific effects (e.g. charge, size). The iRGD- and cRGD-tagged NP formulations showed even higher accumulation in the tumor tissue, demonstrating the additional beneficial effect of specific receptor-ligand binding for tumor-homing. NP accumulation in the tumor was higher than off-target liver accumulation by a factor of ~5 for the non-targeted PEG NPs and a factor of ~8 for the targeted iRGD and cRGD NPs.

In confocal images of tumor tissue, we can see that the NPs penetrate 10-20 μm into surface of the tumor nodules. The iRGD- and cRGD-tagged NPs show a tendency to accumulate on and penetrate (>100 μm) into small tumor nodules (diameter ~300 μm). This preference for binding to small tumor nodules is evidently related to receptor-ligand binding, since there is no such preference for the control PEG NPs. One possibility is that there is a difference in integrin expression between small and large tumor nodules. Regardless of the reason, the

preference of our NP for binding to small tumor nodules is fortunate given that the microscopic tumors are the ones that often evade surgeons and result in cancer recurrence. While we obviously achieved tumor-homing in this study, the expression of our pGFP DNA was fairly low for all samples. However, there are steps we could easily take to improve transfection of these modular CL–NA NPs. Including ionizable lipids or HPEG in our lipid formulation would allow us to maintain low membrane charge density and stealth during delivery and then increase membrane interactions and fusion when the NP is in the late endosome. Both of these options can be easily integrated into future studies.

5. Conclusion

The effective targeting of liposomal carriers to specific tissues is critical for the future of synthetic gene delivery vectors in medicine. By modulating the charge and targeting properties of our peptide-tagged CL–NA NPs, we were able to identify NP formulations *in vitro* that proved to have very good tumor-homing properties *in vivo*. This was achieved using integrin– and NRP-1–binding peptides as tumor-targeting ligands, rather than large antibodies. In this *in vivo* mouse model of peritoneal carcinomatosis, IP-administered CL–NA NPs were able to successfully target and penetrate the microscopic tumors similar to those most likely to cause cancer recurrence in human patients, while also showing very little accumulation in healthy tissue. This demonstrates the utility of the systematic exploration of CL–NA NP formulation space, especially as it concerns the surface charge of the nanoparticle. Both charge ratio and peptide charge were found to be very important in minimizing non-specific charge-mediated binding. In this case, we found that NPs with low membrane charge density and charge ratios near the isoelectric point reduced non-specific cell binding. Both iRGD and cyclic RGD showed very high binding and internalization by multiple cancer cell lines. Surprising, we found that full peptide coverage reduced overall binding, showing that moderation of peptide conjugation maximizes specific ligand-receptor binding. Future work will focus on therapeutic properties of these targeted NPs, which could potentially be achieved with the use of ionizable lipids that increase membrane charge density within late endosomes, facilitating endosomal escape and delivery of the NA cargo.

Acknowledgments

We would like to acknowledge insightful discussions on peptide targeting motifs with Erkki Ruoslahti. This work was supported by the National Institute of Health under Award GM-59288 (C.R.S.), by Cancer Center Support Grant CA30199 from the National Cancer Institute, by Norwegian-Estonian collaboration grant EMP181 (TT), European Research Council starting grant GLIOMADDS from

European Regional Development Fund (TT), and Wellcome Trust International Fellowship WT095077MA (TT). The work was also supported in part by the National Science Foundation under award DMR-1401784 (CRS, zeta-potential). The authors acknowledge the use of the Biological Nanostructures Laboratory within the California NanoSystems Institute, supported by the University of California, Santa Barbara and the University of California, Office of the President. E.W. was supported by the National Science Foundation Graduate Research Fellowship under Grant No. DGE 1144085.

References

[1] Gene Therapy Clinical Trials Worldwide, J. Gene Med. (n.d.). http://www.wiley.com/legacy/wileychi/genmed/clinical/ (accessed May 20, 2010).

[2] X. Guo, L. Huang, Recent advances in nonviral vectors for gene delivery, Acc. Chem. Res. 45 (2012) 971–979. doi:10.1021/ar200151m.

[3] C.R. Safinya, K.K. Ewert, R.N. Majzoub, C. Leal, Cationic liposome–nucleic acid complexes for gene delivery and gene silencing, New J. Chem. 38 (2014) 5164–5172. doi:10.1039/C4NJ01314J.

[4] H. Yin, R.L. Kanasty, A. a Eltoukhy, A.J. Vegas, J.R. Dorkin, D.G. Anderson, Non-viral vectors for gene-based therapy., Nat. Rev. Genet. 15 (2014) 541–555. doi:10.1038/nrg3763.

[5] V.D. Sharma, M.A. Ilies, Heterocyclic cationic gemini surfactants: A comparative overview of their synthesis, self-assembling, physicochemical, and biological properties, Med. Res. Rev. 34 (2014) 1–44. doi:10.1002/med.21272.

[6] W. Bielke, C. Erbacher, eds., Nucleic acid transfection, Springer, Berlin, 2010. doi:10.1016/0302-4598(80)87026-7.

[7] K.K. Ewert, A. Zidovska, A. Ahmad, N.F. Bouxsein, H.M. Evans, C.S. McAllister, C.E. Samuel, C.R. Safinya, Cationic liposome-nucleic acid complexes for gene delivery and silencing: Pathways and mechanisms for plasmid DNA and siRNA, Top. Curr. Chem. 296 (2010) 191–226. doi:10.1007/128_2010_70.

[8] K. Ewert, H.M. Evans, A. Ahmad, N.L. Slack, A.J. Lin, A. Martin-Herranz, C.R. Safinya, Lipoplex Structures and their Distinct Cellular Pathways, in: L. Huang, M.-C. Hung, E. Wagner (Eds.), Non-Viral Vectors Gene Ther. (Advances Genet. Vol. 53), 2nd ed., Elsevier Academic Press, San Diego, 2005: pp. 119–155.

[9] K.K. Ewert, A. Ahmad, H.M. Evans, C.R. Safinya, Cationic lipid-DNA complexes for non-viral gene therapy: Relating supramolecular structures to cellular pathways, Expert Opin. Biol. Ther. 5 (2005) 33–53. doi:10.1517/14712598.5.1.33.

[10] B. Jana, J. Sarkar, P. Mondal, S. Barman, S. Mohapatra, D. Bhunia, K. Pradhan, A. Saha, A. Adak, S. Ghosh, S. Ghosh, A short GC rich DNA derived from microbial origin targets tubulin/microtubules and induces apoptotic death of cancer cells, Chem. Commun. 51 (2015) 12024–12027.

[11] D.A. Williams, C. Baum, Gene therapy - New Challenges Ahead, Science. 302 (2003) 400–401. doi:10.1126/science.1091258.

[12] C.E. Thomas, A. Ehrhardt, M.A. Kay, Progress and problems with the use of viral vectors for gene therapy., Nat. Rev. Genet. 4 (2003) 346–58. doi:10.1038/nrg1066.

[13] S. Hacein-Bey-Abina, A. Garrigue, G.P. Wang, J. Soulier, A. Lim, E. Morillon, E. Clappier, L. Caccavelli, E. Delabesse, K. Beldjord, V. Asnafi, E. MacIntyre, L. Dal Cortivo, I. Radford, N. Brousse, F. Sigaux, D. Moshous, J. Hauer, A. Borkhardt, B.H. Belohradsky, U. Wintergerst, M.C. Velez, L. Leiva, R. Sorensen, N. Wulffraat, S. Blanche, F.D. Bushman, A. Fischer, M. Cavazzana-Calvo, Insertional oncogenesis in 4 patients after retrovirus-mediated gene therapy of SCID-X1, J. Clin. Invest. 118 (2008) 3132–3142. doi:10.1172/JCI35700.

[14] J.O. Rädler, I. Koltover, T. Salditt, C.R. Safinya, Structure of DNA – Cationic Liposome Complexes : DNA Intercalation in Multilamellar Membranes in Distinct Interhelical Packing Regimes, Science. 275 (1997) 810–814. doi:10.1126/science.275.5301.810.

[15] I. Koltover, T. Salditt, C.R. Safinya, Phase diagram, stability, and overcharging of lamellar cationic lipid-DNA self-assembled complexes., Biophys. J. 77 (1999) 915–24. doi:10.1016/S0006-3495(99)76942-0.

[16] A. Ahmad, H.M. Evans, K. Ewert, C.X. George, C.E. Samuel, C.R. Safinya, New multivalent cationic lipids reveal bell curve for transfection efficiency versus membrane charge density: Lipid - DNA complexes for gene delivery, J. Gene Med. 7 (2005) 739–748. doi:10.1002/jgm.717.

[17] A.J. Lin, N.L. Slack, A. Ahmad, C.X. George, C.E. Samuel, C.R. Safinya, Three-dimensional imaging of lipid gene-carriers: membrane charge density controls universal transfection behavior in lamellar cationic liposome-DNA complexes., Biophys. J. 84 (2003) 3307–16. doi:10.1016/S0006-3495(03)70055-1.

[18] A. Ahmad, H.M. Evans, K. Ewert, C.X. George, C.E. Samuel, C.R. Safinya, New multivalent cationic lipids reveal bell curve for transfection efficiency versus membrane charge density: lipid-DNA complexes for gene delivery., J. Gene Med. 7 (2005) 739–48. doi:10.1002/jgm.717.

[19] M.L. Immordino, F. Dosio, L. Cattel, Stealth liposomes: Review of the basic science, rationale, and clinical applications, existing and potential, Int. J. Nanomedicine. 1 (2006) 297–315. doi:10.1023/A:1020134521778.

[20] E. Ruoslahti, S.N. Bhatia, M.J. Sailor, Targeting of drugs and nanoparticles to tumors, J. Cell Biol. 188 (2010) 759–768. doi:10.1083/jcb.200910104.

[21] P.-G. De Gennes, Scaling Concepts in Polymer Physics, 1st ed., Cornell University Press, New York, 1979.

[22] D. Needham, T.J. McIntosh, D.D. Lasic, Repulsive interactions and mechanical stability of polymer-grafted lipid membranes, Biochim. Biophys. Acta - Biomembr. 1108 (1992) 40–48. doi:10.1016/0005-2736(92)90112-Y.

[23] T.L. Kuhl, D.E. Leckband, D.D. Lasic, J.N. Israelachvili, Modulation of interaction forces between bilayers exposing short-chained ethylene oxide headgroups., Biophys. J. 66 (1994) 1479–88. doi:10.1016/S0006-3495(94)80938-5.

[24] R.N. Majzoub, K.K. Ewert, E.L. Jacovetty, B. Carragher, C.S. Potter, Y. Li, C.R. Safinya, Patterned Threadlike Micelles and DNA-Tethered Nanoparticles: A Structural Study of PEGylated Cationic Liposome-DNA Assemblies, Langmuir. 31 (2015) 7073–7083. doi:10.1021/acs.langmuir.5b00993.

[25] A.L. Klibanov, K. Maruyama, V.P. Torchilin, L. Huang, Amphipathic polyethyleneglycols effectively prolong the circulation time of liposomes, FEBS Lett. 268 (1990) 235–237. doi:10.1016/0014-5793(90)81016-H.

[26] G. Blume, G. Cevc, Liposomes for the sustained drug release in vivo., Biochim. Biophys. Acta. 1029 (1990) 91–97. doi:10.1016/0005-2736(90)90440-Y.

[27] D. Papahadjopoulos, T.M. Allen, A. Gabizon, E. Mayhew, K. Matthay, S.K. Huang, K.D. Lee, M.C. Woodle, D.D. Lasic, C. Redemann, Sterically stabilized liposomes: improvements in pharmacokinetics and antitumor therapeutic efficacy., Proc. Natl. Acad. Sci. U. S. A. 88 (1991) 11460–4. doi:10.1073/pnas.88.24.11460.

[28] T.M. Allen, C. Hansen, F. Martin, C. Redemann, A. Yau-Young, Liposomes containing synthetic lipid derivatives of poly(ethylene glycol) show prolonged circulation half-lives in vivo, Biochim. Biophys. Acta - Biomembr. 1066 (1991) 29–36. doi:10.1016/0005-2736(91)90246-5.

[29] M.C. Woodle, D.D. Lasic, Sterically stabilized liposomes, Biochim. Biophys. Acta. 1113 (1992) 171–199. doi:10.1016/0304-4157(92)90038-C.

[30] D. Peer, J.M. Karp, S. Hong, O.C. Farokhzad, R. Margalit, R. Langer, Nanocarriers as an emerging platform for cancer therapy., Nat. Nanotechnol. 2 (2007) 751–760. doi:10.1038/nnano.2007.387.

[31] K.K. Ewert, V.R. Kotamraju, R.N. Majzoub, V.M. Steffes, E.A. Wonder, T. Teesalu, E. Ruoslahti, C.R. Safinya, Synthesis of linear and cyclic peptide–PEG–lipids for stabilization and targeting of cationic liposome–DNA complexes, Bioorg. Med. Chem. Lett. 26 (2016) 1618–1623. doi:10.1016/j.bmcl.2016.01.079.

[32] R. Pasqualini, E. Ruoslahti, Organ targeting in vivo using phage display peptide libraries, Nature. 380 (1996) 364–366. doi:Doi 10.1038/380364a0.

[33] J. Bábíčková, Ľ. Tóthová, P. Boor, P. Celec, In vivo phage display - A discovery tool in molecular biomedicine, Biotechnol. Adv. 31 (2013) 1247–1259. doi:10.1016/j.biotechadv.2013.04.004.

[34] T. Teesalu, K.N. Sugahara, E. Ruoslahti, Mapping of vascular ZIP codes by phage display, Methods Enzymol. 503 (2012) 35–56. doi:10.1016/B978-0-12-396962-0.00002-1.

[35] E. Ruoslahti, D. Rajotte, An address system in the vasculature of normal tissues and tumors., Annu. Rev. Immunol. 18 (2000) 813–27. doi:10.1146/annurev.immunol.18.1.813.

[36] E. Ruoslahti, Vascular zip codes in angiogenesis and metastasis., Biochem. Soc. Trans. 32 (2004) 397–402. doi:10.1042/BST0320397.

[37] E. Ruoslahti, T. Duza, L. Zhang, Vascular homing peptides with cell-penetrating properties., Curr. Pharm. Des. 11 (2005) 3655–60. doi:10.2174/138161205774580787.

[38] L. Simón-Gracia, H. Hunt, P. Scodeller, J. Gaitzsch, V.R. Kotamraju, K.N. Sugahara, O. Tammik, E. Ruoslahti, G. Battaglia, T. Teesalu, iRGD peptide conjugation potentiates intraperitoneal tumor delivery of paclitaxel with polymersomes, Biomaterials. 104 (2016) 247–257. doi:10.1016/j.biomaterials.2016.07.023.

[39] J. Rieger, W. Wick, M. Weller, Human malignant glioma cells express semaphorins and their receptors, neuropilins and plexins, Glia. 42 (2003) 379–389. doi:10.1002/glia.10210.

[40] a Meyer, J. Auernheimer, a Modlinger, H. Kessler, Targeting RGD recognizing integrins: drug development, biomaterial research, tumor imaging and targeting., Curr. Pharm. Des. 12 (2006) 2723–2747. doi:10.2174/138161206777947740.

[41] E. Ruoslahti, S.N. Bhatia, M.J. Sailor, Targeting of drugs and nanoparticles to tumors, J. Cell Biol. 188 (2010) 759–768. doi:10.1083/jcb.200910104.

[42] M.D. Pierschbacher, E. Ruoslahti, Cell attachment activity of fibronectin can be duplicated by small synthetic fragments of the molecule, Nature. 309 (1984) 30–33. doi:10.1038/309030a0.

[43] E. Ruoslahti, M.D. Pierschbacher, Arg-Gly-Asp: a versatile cell recognition signal., Cell. 44 (1986) 517–518. doi:10.1016/0092-8674(86)90259-X.

[44] E. Koivunen, D. a Gay, E. Ruoslahti, Selection of peptides binding to the alpha 5 beta 1 integrin from phage display library., J. Biol. Chem. 268 (1993) 20205–10.

[45] M. Gurrath, G. Muller, H. Kessler, M. Aumailley, R. Timpl, Conformation/activity studies of rationally designed potent anti-adhesive RGD peptides, Eur. J. Biochem. 210 (1992) 911–921. doi:10.1111/j.1432-1033.1992.tb17495.x.

[46] H. Kessler, B. Diefenbach, D. Finsinger, A. Geyer, M. Gurrath, S.L. Goodman, G. Hölzemann, R. Haubner, A. Jonczyk, G. Müller, E.G. von Roedern, J. Wermuth, Design of superactive and selective integrin receptor antagonists containing the RGD sequence, Lett. Pept. Sci. 2 (1995) 155–160. doi:10.1007/BF00119142.

[47] K.N. Sugahara, T. Teesalu, P.P. Karmali, V.R. Kotamraju, L. Agemy, D.R. Greenwald, E. Ruoslahti, Coadministration of a Tumor-Penetrating Peptdei Enhances the Efficacy of Cancer Drugs, Science 328 (2010) 1031–1038. doi:10.1007/s13398-014-0173-7.2.

[48] A.-M.A. Willmore, L. Simón-Gracia, K. Toome, P. Paiste, V.R. Kotamraju, T. Mölder, K.N. Sugahara, E. Ruoslahti, G.B. Braun, T. Teesalu, Targeted silver nanoparticles for ratiometric cell phenotyping, Nanoscale. 8 (2016) 9096–9101. doi:10.1039/C5NR07928D.

[49] K.N. Sugahara, T. Teesalu, P.P. Karmali, V.R. Kotamraju, L. Agemy, O.M. Girard, D. Hanahan, R.F. Mattrey, E. Ruoslahti, Tissue-Penetrating Delivery of Compounds and Nanoparticles into Tumors, Cancer Cell. 16 (2009) 510–520. doi:10.1016/j.ccr.2009.10.013.

[50] K.N. Sugahara, P. Scodeller, G.B. Braun, T.H. De Mendoza, C.M. Yamazaki, M.D. Kluger, J. Kitayama, E. Alvarez, S.B. Howell, T. Teesalu, E. Ruoslahti, A.M. Lowy, A tumor-penetrating peptide enhances circulation-independent targeting of peritoneal carcinomatosis, J. Control. Release. 212 (2015) 59–69. doi:10.1016/j.jconrel.2015.06.009.

[51] C. Puig-Saus, L. Rojas, E. Laborda, A. Figueras, R. Alba, C. Fillat, R. Alemany, iRGD tumor-penetrating peptide-modified oncolytic adenovirus shows enhanced tumor transduction, intratumoral dissemination and antitumor efficacy, Gene Ther. 21 (2014) 767–774. doi:10.1038/gt.2014.52.

[52] K. Wang, X. Zhang, Y. Liu, C. Liu, B. Jiang, Y. Jiang, Tumor penetrability and anti-angiogenesis using iRGD-mediated delivery of doxorubicin-polymer conjugates, Biomaterials. 35 (2014) 8735–8747. doi:10.1016/j.biomaterials.2014.06.042.

[53] G. Gu, X. Gao, Q. Hu, T. Kang, Z. Liu, M. Jiang, D. Miao, Q. Song, L. Yao, Y. Tu, Z. Pang, H. Chen, X. Jiang, J. Chen, The influence of the penetrating peptide iRGD on the effect of paclitaxel-loaded MT1-AF7p-conjugated nanoparticles on glioma cells, Biomaterials. 34 (2013) 5138–5148. doi:10.1016/j.biomaterials.2013.03.036.

[54] Y. Akashi, T. Oda, Y. Ohara, R. Miyamoto, T. Kurokawa, S. Hashimoto, T. Enomoto, K. Yamada, M. Satake, N. Ohkohchi, Anticancer effects of gemcitabine are enhanced by co-administered iRGD peptide in murine pancreatic cancer models that overexpressed neuropilin-1., Br. J. Cancer. 110 (2014) 1481–7. doi:10.1038/bjc.2014.49.

[55] L. Agemy, D. Friedmann-Morvinskib, V.R. Kotamrajua, L. Rotha, K.N. Sugaharac, O.M. Girardd, R.F. Mattreyd, I.M. Vermab, E. Ruoslahti, Targeted nanoparticle enhanced proapoptotic peptide as potential therapy for glioblastoma, Proc. Natl. Acad. Sci. U. S. A. 108 (2011) 17450–17455. doi:10.1073/pnas.1114518108/.

[56] C. Schmithals, V. Köberle, H. Korkusuz, T. Pleli, B. Kakoschky, E.A. Augusto, A.A. Ibrahim, J.M. Arencibia, V. Vafaizadeh, B. Groner, H.W. Korf, B. Kronenberger, S. Zeuzem, T.J. Vogl, O. Waidmann, A. Piiper, Improving drug penetrability with iRGD leverages the therapeutic response to sorafenib and doxorubicin in hepatocellular carcinoma, Cancer Res. 75 (2015) 3147–3154. doi:10.1158/0008-5472.CAN-15-0395.

[57] H.-B. Pang, G.B. Braun, T. Friman, P. Aza-Blanc, M.E. Ruidiaz, K.N. Sugahara, T. Teesalu, E. Ruoslahti, An endocytosis pathway initiated through neuropilin-1 and regulated by nutrient availability, Nat. Commun. 5 (2014) 4904. doi:10.1038/ncomms5904.

[58] D.D. Lasic, D. Papahadjopoulos, INTRAPERITONEAL CANCER THERAPY: PRINCIPLES AND PRACTICE, CRC Press, Boca Ratan, FL, USA, 2015.

[59] G. Montori, F. Coccolini, M. Ceresoli, F. Catena, N. Colaianni, E. Poletti, L. Ansaloni, The treatment of peritoneal carcinomatosis in advanced gastric cancer: State of the art, Int. J. Surg. Oncol. 2014 (2014) 912418. doi:10.1155/2014/912418.

[60] Y.L.B. Klaver, V.E.P.P. Lemmens, S.W. Nienhuijs, M.D.P. Luyer, I.H.J.T. de Hingh, Peritoneal carcinomatosis of colorectal origin: Incidence, prognosis and treatment options, World J. Gastroenterol. 18 (2012) 5489–5494. doi:10.3748/wjg.v18.i39.5489.

[61] R. Eskander, L. Ansaloni, R. Bristow, F. Coccolini, Cytoreductive surgery and hyperthermic intraperitoneal chemotherapy in epithelial ovarian cancer: State of the art., World J. Obs. Gynecol. 2 (2013) 94–100. doi:10.5317/wjog.v2.i4.94.

[62] M. Tsai, Z. Lu, J. Wang, T.K. Yeh, M.G. Wientjes, J.L.S. Au, Effects of carrier on disposition and antitumor activity of intraperitoneal paclitaxel, Pharm. Res. 24 (2007) 1691–1701. doi:10.1007/s11095-007-9298-0.

[63] I. Königsrainer, P. Horvath, F. Struller, V. Forkl, A. Königsrainer, S. Beckert, Risk factors for recurrence following complete cytoreductive surgery and HIPEC in colorectal cancer-derived peritoneal surface malignancies, Langenbeck's Arch. Surg. 398 (2013) 745–749. doi:10.1007/s00423-013-1065-6.

[64] K. Ewert, A. Ahmad, H.M. Evans, H.W. Schmidt, C.R. Safinya, Efficient synthesis and cell-transfection properties of a new multivalent cationic lipid for nonviral gene delivery, J. Med. Chem. 45 (2002) 5023–5029. doi:10.1021/jm020233w.

[65] U. Schulze, H. Schmidt, C.R. Safinya, Synthesis of Novel Cationic Poly (Ethylene Glycol) Containing Lipids, Bioconjugate Chem. 10 (1999) 548–552.

[66] A. Koga, K. Aoyagi, T. Imaizumi, M. Miyagi, K. Shirouzu, Comparison between the gastric cancer cell line MKN-45 and the high-potential peritoneal dissemination gastric cancer cell line MKN-45P., Kurume Med.

J. 58 (2011) 73–9. doi:10.2739/kurumemedj.58.73.

[67] M. Sutherland, A. Gordon, S.D. Shnyder, L.H. Patterson, H.M. Sheldrake, RGD-binding integrins in prostate cancer: Expression patterns and therapeutic prospects against bone metastasis, Cancers 4 (2012) 1106–1145. doi:10.3390/cancers4041106.

[68] S. Roy, J.Y. Axup, J.S. Forsyth, R.K. Goswami, B.M. Hutchins, K.M. Bajuri, S.A. Kazane, V. V. Smider, B.H. Felding, S.C. Sinha, SMI-Ribosome inactivating protein conjugates selectively inhibit tumor cell growth, Chem. Commun. (2017). doi:10.1039/C7CC00745K.

[69] C.-L. Chan, R.N. Majzoub, R.S. Shirazi, K.K. Ewert, Y.-J. Chen, K.S. Liang, C.R. Safinya, Endosomal escape and transfection efficiency of PEGylated cationic liposome-DNA complexes prepared with an acid-labile PEG-lipid., Biomaterials. 33 (2012) 4928–35. doi:10.1016/j.biomaterials.2012.03.038.